Hindawi
PPAR Research
Volume 2023, Article ID 8047378, 15 pages
https://doi.org/10.1155/2023/8047378

Research Article

Peptide Helix-Y^{12} as Potential Effector for Peroxisome Proliferator-Activated Receptors

Mauricio Carrillo-Tripp,[1] **Yair Reyes**,[2,3] **Blanca Delgado-Coello**,[4] **Jaime Mas-Oliva**,[4] **and Roxana Gutiérrez-Vidal**[2,5]

[1]*Biomolecular Diversity Laboratory, Centro de Investigación y de Estudios Avanzados del Instituto Politécnico Nacional, Unidad Monterrey, Vía del Conocimiento 201, PIIT, C.P. 66600, Apodaca, Nuevo León, Mexico*
[2]*Metabolic Diseases Laboratory, Centro de Investigación y de Estudios Avanzados del Instituto Politécnico Nacional, Unidad Monterrey, Vía del Conocimiento 201, PIIT, C.P. 66600, Apodaca, Nuevo León, Mexico*
[3]*Universidad Politécnica de Puebla, Tercer Carril del Ejido, Serrano s/n, Cuanalá, C.P. 7264, Puebla, Mexico*
[4]*Instituto de Fisiología Celular, Universidad Nacional Autónoma de México, C.P. 04510, CDMX, Mexico*
[5]*Programa de Investigadoras e Investigadores por México, Conacyt, CDMX, Mexico*

Correspondence should be addressed to Roxana Gutiérrez-Vidal; roxana.gutierrezv@cinvestav.mx

Received 17 October 2022; Revised 29 March 2023; Accepted 3 April 2023; Published 15 April 2023

Academic Editor: Antonio Brunetti

Peroxisome proliferator-activated receptors (PPARs) are nuclear receptors involved in the regulation of lipids and glucose metabolism, and immune response. Therefore, they have been considered pharmacological targets for treating metabolic diseases, such as dyslipidemia, atherosclerosis, and non-alcoholic fatty liver disease. However, the available synthetic ligands of PPARs have mild to significant side effects, generating the necessity to identify new molecules that are selective PPAR ligands with specific biological responses. This study aimed to evaluate some components of the atheroprotective and hepatoprotective HB-ATV-8 nanoparticles [the amphipathic peptide Helix-Y^{12}, thermozeaxanthin, thermozeaxanthin-13, thermozeaxanthin-15, and a set of glycolipids], as possible ligands of PPARs through blind molecular docking. According to the change in free energy upon protein–ligand binding, ΔG_b, thermozeaxanthins show a more favorable interaction with PPARs, followed by Helix-Y^{12}. Moreover, Helix-Y^{12} interacts with most parts of the Y-shaped ligand-binding domain (LBD), surrounding helix 3 of PPARs, and reaching helix 12 of PPARα and PPARγ. As previously reported for other ligands, Tyr314 and Tyr464 of PPARα interact with Helix-Y^{12} through hydrogen bonds. Several PPARα's amino acids are involved in the ligand binding by hydrophobic interactions. Furthermore, we identified additional PPARs' amino acids interacting with Helix-Y^{12} through hydrogen bonds still not reported for known ligands. Our results show that, from the studied ligand set, the Helix-Y^{12} peptide and Tzeaxs have the most significant probability of binding to the PPARs' LBD, suggesting novel ligands for PPARs.

1. Introduction

Peroxisome proliferator-activated receptors (PPARs) are ligand-activated transcription factors that regulate genes involved in several biological processes, mainly glucose and lipid metabolism, as well as immune response. This family of nuclear receptors includes the isoforms PPARα, PPARβ/δ, and PPARγ, each encoded by a different gene located on separate chromosomes, but with a high degree of sequence and structural homology [1].

Tissue distribution patterns and expression levels are the main differences between the three isoforms, displaying regulatory activities and modulating specific responses [2]. PPARα is expressed predominantly in skeletal muscle, heart, liver, and brown adipose tissue, all of them are high-energy-requiring tissues. There is also an important expression of PPARα in cells composing the vasculature, such as endothelial cells, smooth muscle cells, and monocytes/macrophages [3–6]. PPARγ is highly expressed in adipose tissue and macrophages, and at much lower levels in the liver and muscle.

This isoform has been considered as a master regulator of adipogenesis, lipid storage, insulin sensitivity, and immune regulation. Moreover, the expression of PPARα and PPARγ in the subendothelial region and the lipid core of atherosclerotic lesions, where they colocalize with specific markers of macrophages, smooth muscle cells, and foam cells, has been described [7]. PPARβ/δ, the third family member, shows expression in a variety of tissues, such as heart, vascular smooth muscle cells, adipose tissue, brain, intestine, muscle, spleen, lung, and adrenal glands [8].

The tertiary structure of the PPARs has a DNA binding domain in the N-terminus and a ligand-binding domain (LBD) in the C-terminus. The LDB is a Y-shaped pocket composed of 13 α-helices and 4 β-sheets. This pocket contains the activation function (AF-2) region that serves as a binding site for coregulator proteins [9], and the helix H12 is considered as the activating site [10]. The dynamic conformation of LBD is stabilized with PPAR ligand binding, promoting interactions with coregulator proteins, in turn remodeling the chromatin, facilitating polymerase binding, and expression of target genes [9]. Although, ligand-dependent transactivation of PPARs is one of their mechanisms; they also present ligand-independent repression and ligand-dependent transrepression [11, 12].

The main ligands for PPARs are endogenous lipid-soluble fatty acids and their derivatives, such as eicosanoids, prostaglandins, and leukotriene B4 [13]. Examples of these fatty acids that interact in LBD are conjugated linoleic acid, 9-(s)-hydroxyoctadecadienoic, and 15-deoxydelta12,14-prostaglandin J12, which are known endogenous and dietary agonists [14]. Ligands can also be synthetic, such as Wy-14643 and fibrates (specific PPARα activators) [13]. The latter have proven to increase triglyceride catabolism through overexpression of lipoprotein lipase and reduce the secretion of chylomicrons in enterocytes. They also increase circulating levels of atheroprotective high-density lipoprotein cholesterol [15], and improve the overall atherogenic plasma lipid profile. GW501516 is a highly-selective PPARβ/δ ligand, and thiazolidinedione (TZD) derivatives (troglitazone, pioglitazone, GW1929, and GW2090) are specific PPARγ activators [13]. In the vasculature, PPARs agonists have a role in vascular metabolism involved in recruitment and adhesion of inflammatory cells. They also induce nitric oxide synthase expression by increasing nitric oxide bioavailability, suggesting vasculoprotective effects [16, 17]. Furthermore, PPARα increases the expression of IκB, an inhibitor of the pro-inflammatory transcription factor nuclear factor κ beta (NF-κB). It also inhibits many inflammatory genes, such as NF-κB, activator protein 1, and nuclear factor of activated T cells by transrepression. PPARα activation reduces the production of proinflammatory cytokines, such as interleukin-1 and interleukin-6, thus preventing the expression of adhesion molecules, such as vascular cell adhesion molecule-1 and intracellular cell adhesion molecule-1 [18–20]. In mice, PPARα activation using fibrates proved to be protective for acute liver injury [21]. TZDs are potent PPARγ agonists that increase insulin sensitivity and induce browning of white fat [22]. Furthermore, activation of PPARγ by a TZD (pioglitazone) has vascular protective action explained through ligand-dependent formation of the complex of PPARγ–high mobility group A1-SUMO E2 ligase Ubc9 that promote PPARγ SUMOylation, necessary for the metalloproteinase-9 transrepression, a key mediator of vascular injury [12]. However, TZDs are associated with several side effects, including gain in body weight and visceral obesity. Selective PPARγ modulators (amorfrutins) have been shown to improve insulin sensitivity, dyslipidemia [23], liver steatosis [24], and atherosclerosis [25], without increasing body weight. It has been shown that a partial activator of PPARγ, telmisaten, in combination with activating PPARα in the liver, could alleviate hepatic steatosis in mice that were fed a high-fat diet [26]. According to the literature, PPAR agonists are suitable drug targets for treating highly prevalent metabolic diseases, such as type 2 diabetes, atherosclerosis, and non-alcoholic fatty liver disease (NAFLD). However, given the low efficacy and side effects of current PPAR agonists, there is a need for the development or identification of new molecules that are safe and selective PPAR ligands to obtain a more specific agonist activity to promote selected biological responses [27, 28].

We have previously shown that HB-ATV-8 lipid nanoparticles have a protective effect against atherosclerotic lesions and NAFLD induced by a high-fat diet in pigs and rabbits [29, 30]. The nanoparticles are mainly composed of membrane lipids of *Thermus aquaticus* and an amphipathic peptide (Cys+ the last 11 residues of the cholesteryl-ester transfer protein, called Helix-Y^{12}). The HB-ATV-8 nanoparticles induce mild cholesteryl-ester transfer protein antibodies production, explaining in part the observed effect. However, the protective effect is present even without antibody production [29]. Hence, we suggest that peptide Helix-Y^{12} and the lipid components of the nanoparticles could participate directly in the biological effect. The membrane of *T. aquaticus* has abundant carotenoids, such as thermozeaxanthins (Tzeaxs), glycolipids, and glycerophospholipids. Carotenoids have antioxidant properties, also reported as bioactive lipids that bind to receptors and transcription factors modifying several related-pathways, lipids, and inflammation [31–35].

In this study, we evaluate a set of molecules found in the HB-ATV-8 formulation, namely, the Helix-Y^{12} peptide and main lipids from the membrane of *T. aquaticus*, to identify potential effectors of PPARα, PPARβ/δ, and PPARγ based on the change in free energy after protein–ligand binding and the types of interactions found through blind molecular coupling. Our results show that the peptide Helix-Y^{12} and the Tzeaxs establish favorable interactions with the LBD of the three PPARs. However, the peptide establishes more hydrogen bonds than some Tzeaxs, forming a clamp inside the PPARs LBD reaching H3 and H12 helices. These findings shed light into the mechanisms of action of the nanoparticles that protect against atherosclerotic and hepatic lesions induced by a high-fat diet.

2. Methods

2.1. Target and Ligand Molecular Modeling. The three-dimensional coordinates of the crystallographic structure of

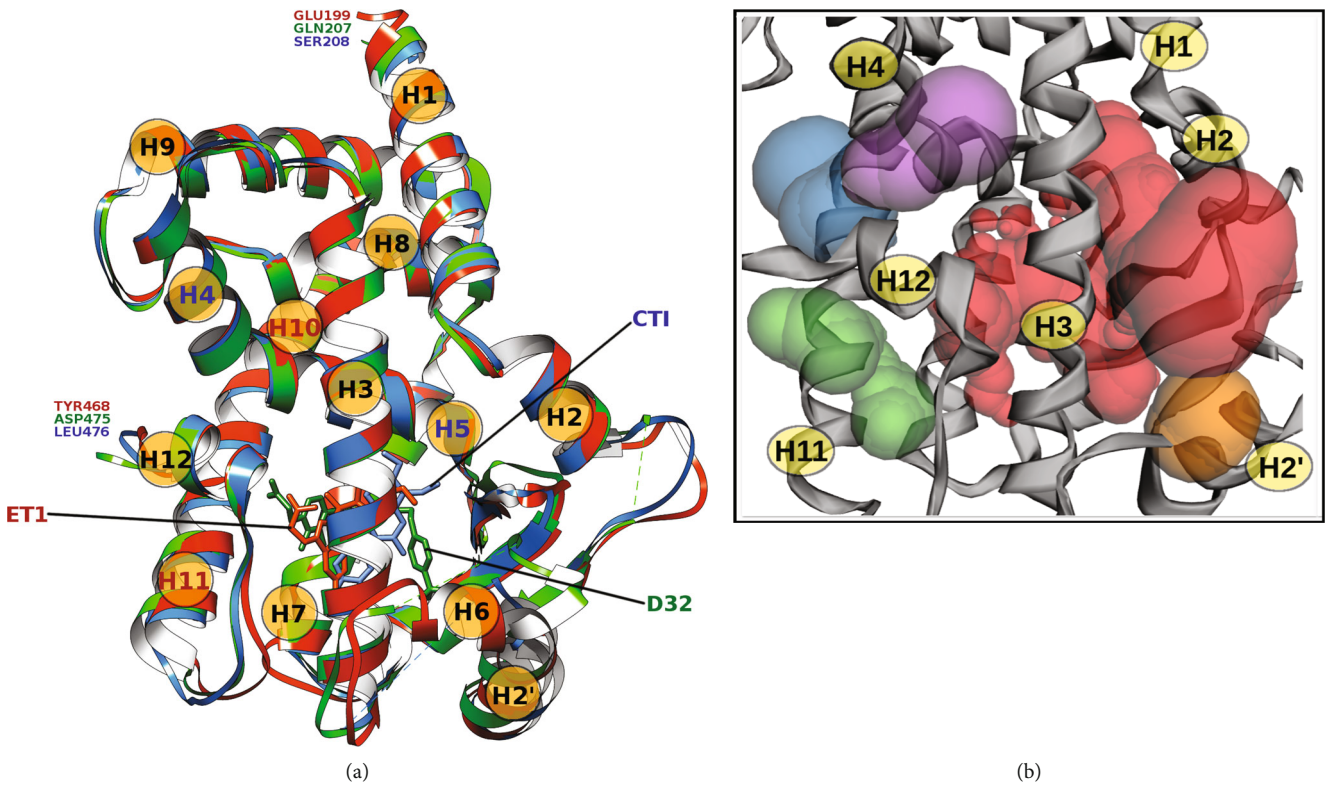

Figure 1: Molecular structure of protein targets: (a) co-crystallized in complex with a corresponding active molecule in the LBD (holo state) PPARα-ET1 (PDBID: 3ET1, in red), PPARβ/δ-D32 (PDBID: 3GZ9, in green), and PPARγ-CTI (PDBID: 4Y29, in blue). (b) Top 5 cavities, ranked by size, LBD in red 458 Å^3, green 63 Å^3, blue 52 Å^3, purple 42 Å^3, and orange 1 Å^3 (volumes calculated with the CASTp 3.0 [76] on 3GZ9). Helix pairs H4–H5 and H10–H11 are continuous secondary structures.

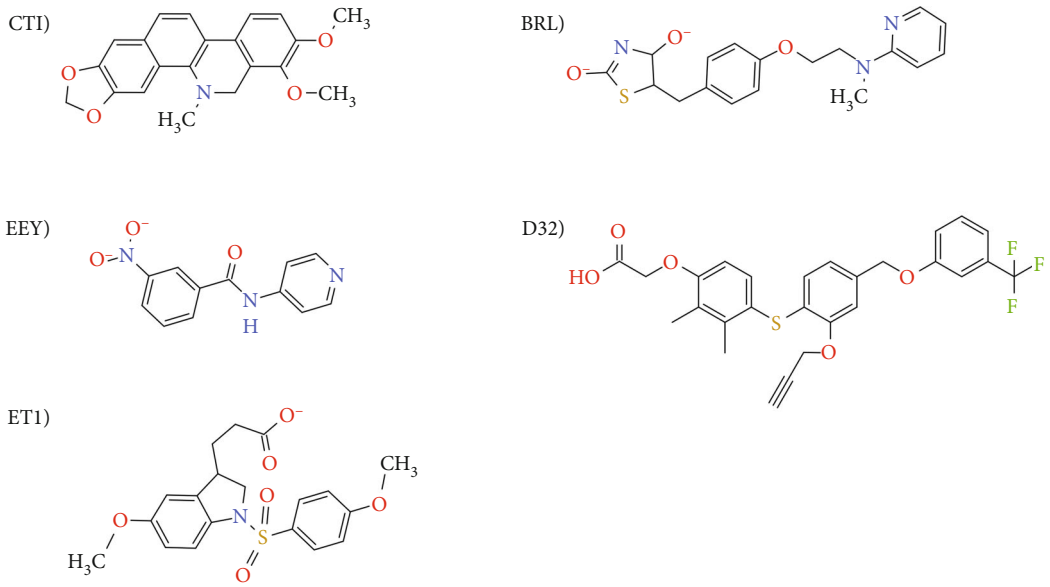

Figure 2: Chemical structure of the active molecules in the positive control group used in the molecular docking: ET1 for PPARα, D32 for PPARβ/δ, and CTI, EEY, and BRL for PPARγ.

PPARα (PDBID: 3ET1), PPARβ/δ (PDBID: 3GZ9), and PPARγ (PDBID: 4Y29) were obtained from the RCSB PDB database [36], shown in Figure 1. Structural data curation involved deleting solvent and non-complexed ions, keeping the highest occupancy atom locations, replacing incomplete side chains using the Dunbrack 2010 rotamers, and adding hydrogen atoms, using the Chimera's Dock Prep tools v 1.13.1 [37, 38]. We built a positive control group composed

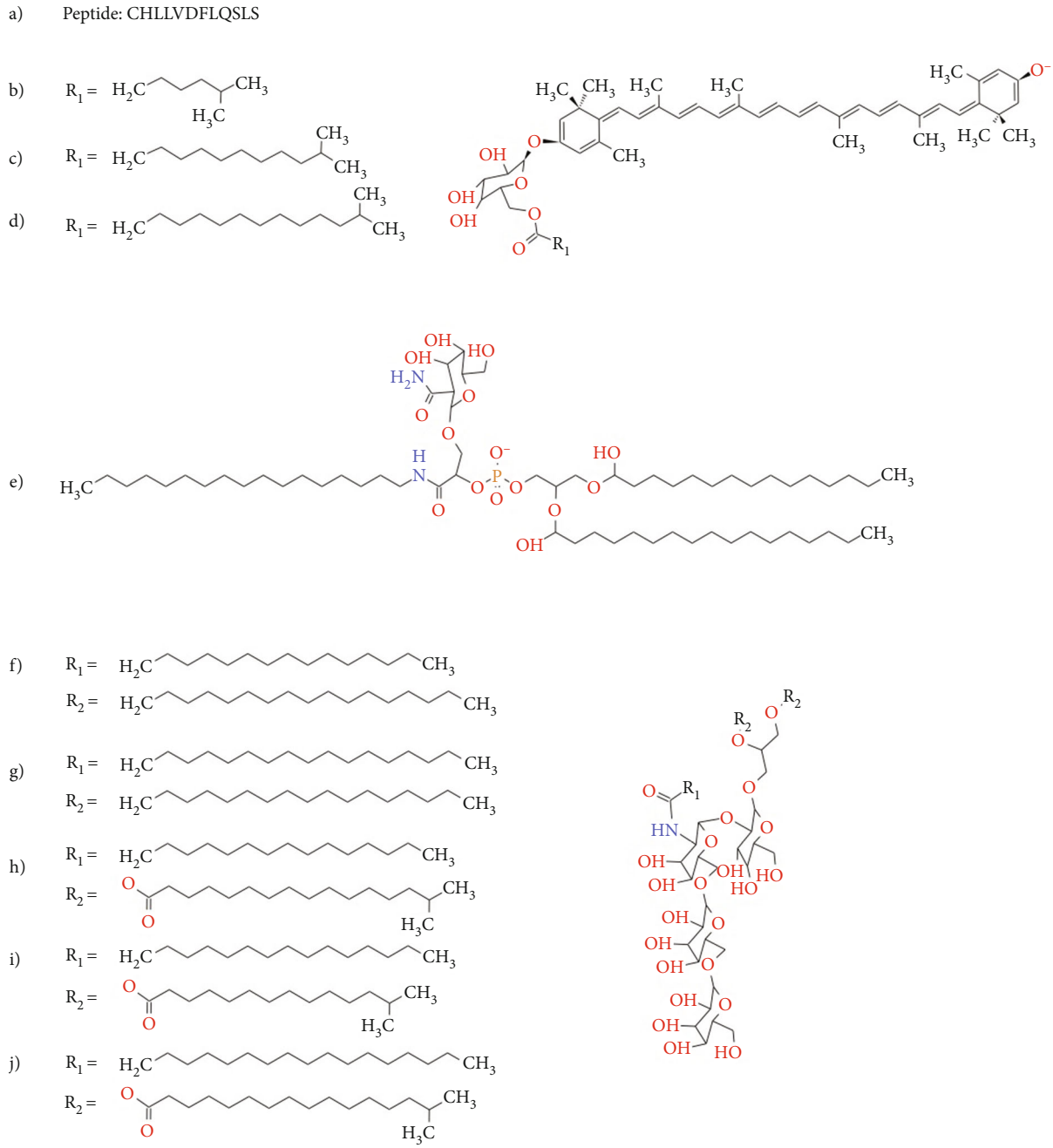

Figure 3: Chemical structure of the ligand molecules in the experimental group used for molecular docking: (a) Helix-Y[12], (b) Tzeax, (c) Tzeax-13, (d) Tzeax-15, (e) gpl01, (f) gl01, (g) gl02, (h) gl03, (i) gl04, and (j) gl05.

of the ligands found in the co-crystallization experiments of the target molecules to validate the blind molecular docking methodology is shown in Figure 2.

Given the results reported in a previous study [39], we analyzed the interaction between PPARs and the 12 amino acids long amphipathic peptide, Helix-Y[12]. In addition, we included relevant components of HB-ATV-8 nanoparticles to build the experimental set of ligands is shown in Figure 3, because it is well known that PPARs are promiscuous toward lipids and their derivatives. Nanoparticles are composed of lipids from *T. aquaticus* cell's membrane, which contains phospholipids, glycolipids, and carotenoids. In this study, we selected the carotenoids Tzeax, thermozeaxanthin-13 (Tzeax-13), and thermozeaxanthin-15 (Tzeax-15) due to their high abundance in the *T. aquaticus* lipid membrane and their antioxidant properties, as well as some representative glycerophospholipids.

In all cases, the molecular structure of the ligands was built from scratch based on their chemical structure (Figures 2 and 3) using the Chimera v 1.13.1 [37]. After adding Gasteiger partial charges on all atoms based on the Amber 14SB force-field, a two-step minimization phase was done carrying out 3,000 steepest descent and 10,000 conjugate gradient steps with a 0.02 step size in both cases. The minimized structure was exported in MOL2 format and imported into the AutoDockTools v1.5.6

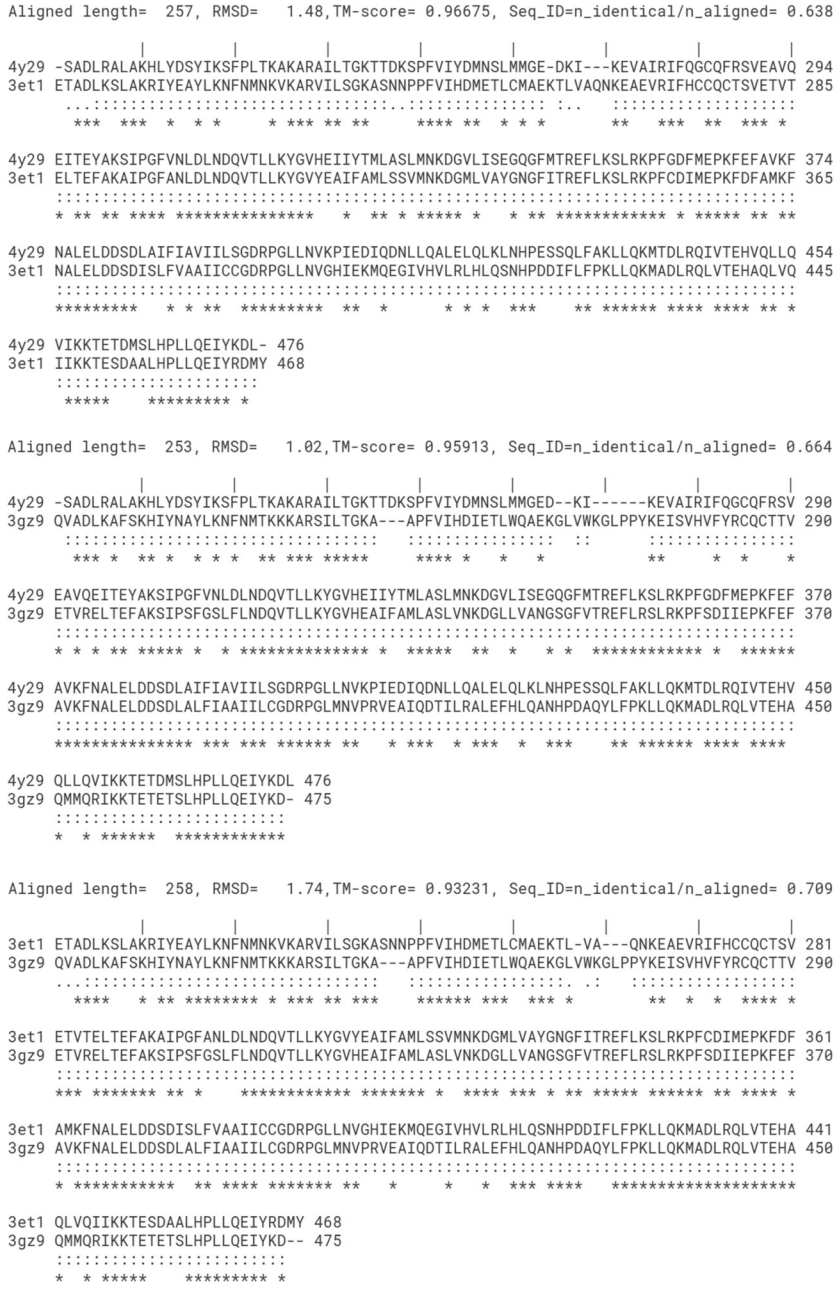

FIGURE 4: Structure-based sequence alignment of the three PPAR variants. Top to bottom: PPARγ (PDBID 4y29) versus PPARα (PDBID 3et1), PPARγ (PDBID 4y29) versus PPARβ/δ (PDBID 3gz9), and PPARα (PDBID 3et1) versus PPARβ/δ (PDBID 3gz9). For each pair of variants, aligned length, RMSD, TM-score, and sequence identity were reported using the TM-align algorithm. For each aligned residue pair, ":" denotes distance $<5:0$ Å, "." denotes farther aligned residues, and "*" denotes identical residues.

through the Ligand-input menu. All non-polar hydrogen atoms were merged with corresponding carbon atoms automatically, leaving only explicit polar hydrogen atoms, also detecting rotatable bonds (torsion degrees of freedom). At the end, the ligands molecular structures were exported in PDBQT format.

2.2. Protein–Ligand Blind Molecular Docking. After the target and ligand molecular modeling, a three-phase pipeline cycle was followed: target cavity detection, docking box optimization, and target–ligand docking. An in-house bash script was developed (https://github.com/tripplab/HTVS) [40] to implement and automatize the CB-Dock [41] and the AutoDock Vina [42] computational tools in a high-throughput fashion at a local high-performance computing multi-core server. Since CB-Dock is a cavity detection-guided protein–ligand blind docking, the curated target tertiary structure was analyzed to find all cavities in the protein's surface. This was accomplished by the CurPocket tool, which is based on a curvature-dependent surface-area model [43]. All detected cavities were ranked by surface area size, from largest to smallest. The ligand structure data and the location and size of the cavities found in the

Table 1: Structural comparison of PPARs. Root mean square deviation [Å], protein fold similarity, and sequence identity [%]. All metrics evaluated with the TM-align tool [45].

PPAR	RMSD	TM-score	Seq id
α–δ	1.74	0.93	0.71
α–γ	1.48	0.97	0.64
δ–γ	1.02	0.96	0.66

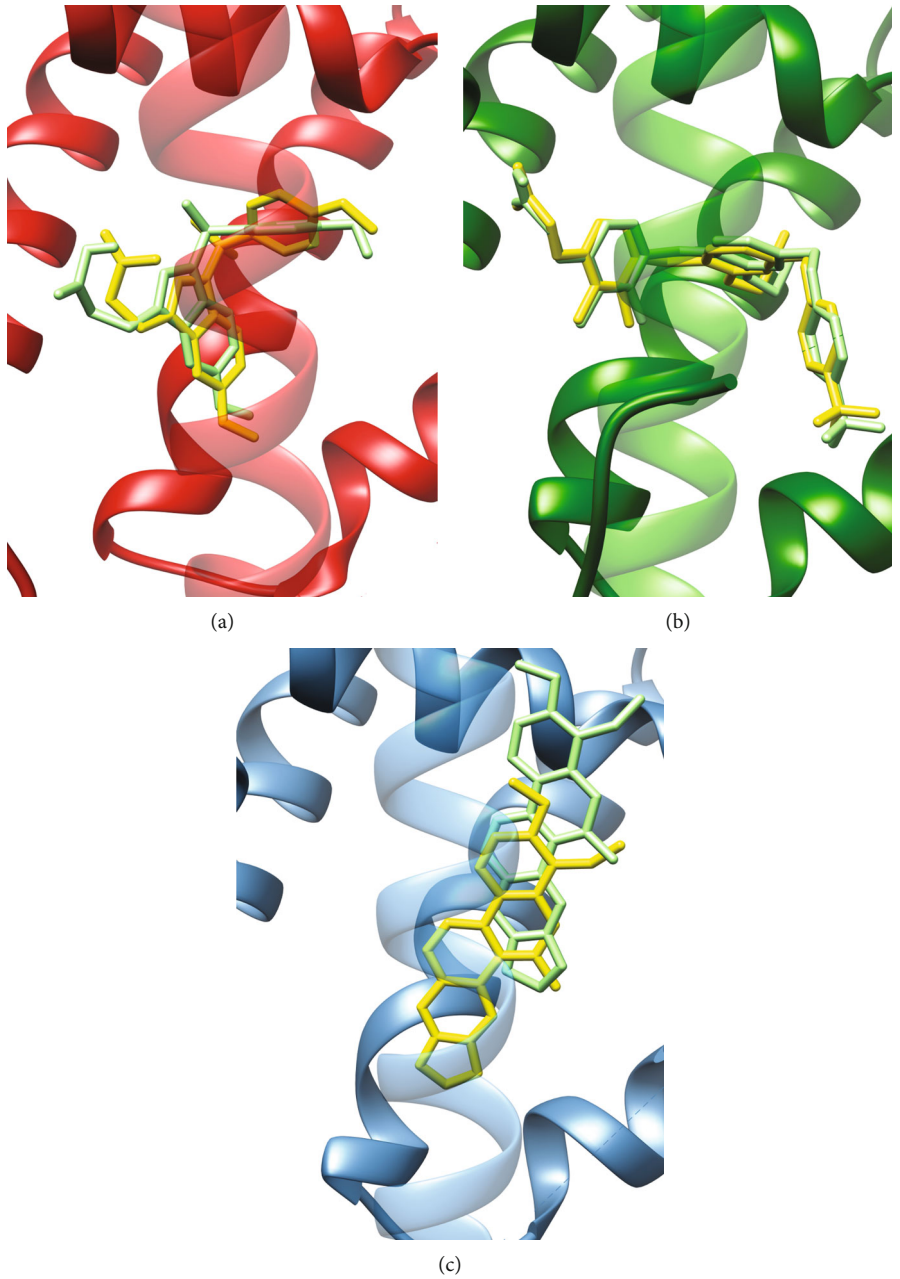

Figure 5: Results for the active molecules in the positive control group: (a) ET1 for PPARα (in red), (b) D32 for PPARβ/δ (in green), and (c) CTI for PPARγ (in blue). In all cases, co-crystalized ligand in yellow, blind docking prediction in green, and PPAR helix H3 transparent.

target's molecular surface were used to define a customized docking box, which was used as input parameters in the next phase. The AutoDock Vina has been shown to be a fast and accurate docking method based on a free energy scoring function that allows for efficient optimization and multithreading. It takes the PDBQT target and ligand

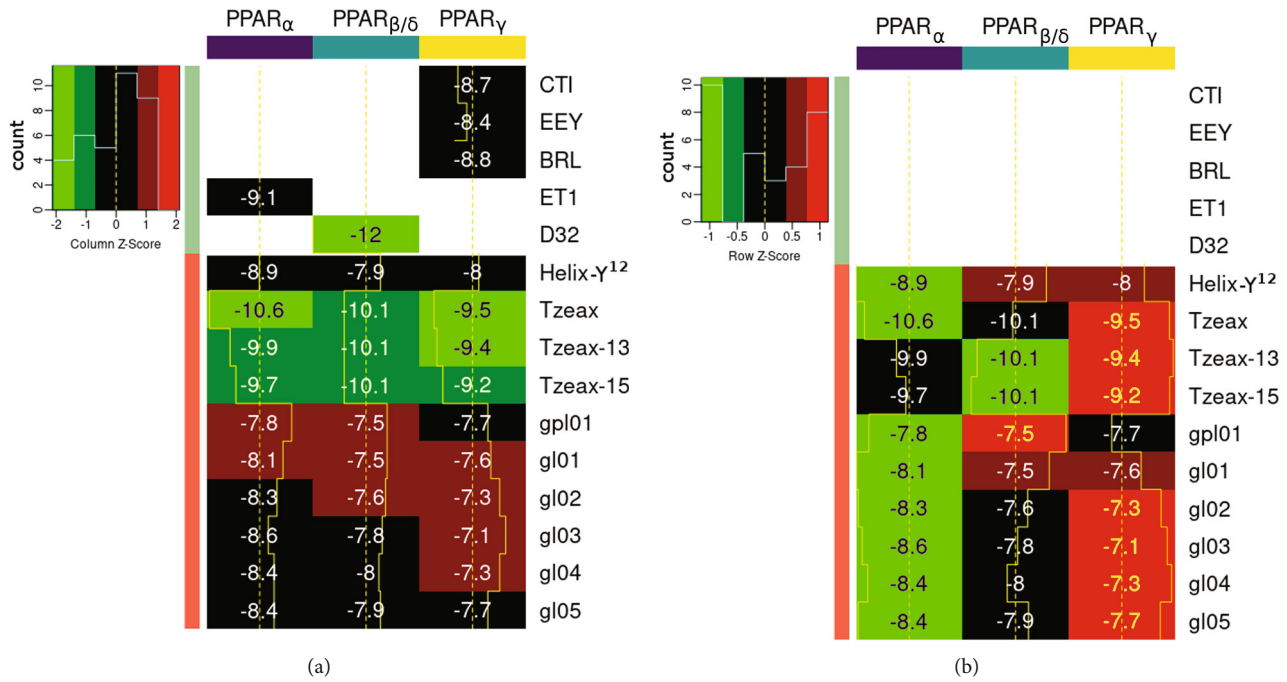

FIGURE 6: Target–ligand ΔG_b values (kcal/mol) at the biologically active cavity of PPARα (purple), PPARβ/δ (blue), and PPARγ (yellow). Statistical Z-score analysis heat-map (a) for the ligand set (columns) and (b) for the target set (rows).

structural data as inputs, as well as the docking box configuration optimized parameters.

For a full virtual screening, we provided the set of targets T and the set of ligands L (PDBQTs), the number of target cavities to sample N, and the number of independent rounds K to perform for each target–ligand pair. As a result, the pipeline outputs a numeric matrix with the change in binding free energy values ΔG_b for all target–ligand top conformations for each cavity into a database. The data was analyzed with the *heatmap.2(data.matrix(sheet))* R function. The rows and columns were independently scaled to have *mean* = 0 and *standard deviation* = 1 to generate two Z-score based heat-map representations of the data. Furthermore, two-dimensional diagrams from the predicted protein–ligand complexes were generated using the Ligplot [44] to identify the PPARs LBD amino acids involved in the favorable interaction with the corresponding ligand.

3. Results and Discussion

The structural superposition of the three LBD of the PPARs (Figure 1(a)) shows that the pair-wise Cα Root Mean Square Deviation (RMSD) is below 2 Å and the TM-score is above 0.9, indication that they share the same protein fold. However, the sequence identity is relatively low (Figure 4), hence, we considered them as three independent targets for the molecular docking (Table 1).

For every target–ligand pair, we ran consecutive independent blind molecular docking cycles, each one sampling the top 5 cavities detected on the surface of the target (Figure 1(b)). We continued running cycles until we no longer found lower ΔG_b values, suggesting a sufficiently large sampling of the conformational space. We found that 20 independent cycles for each pair were enough. We then selected the conformation with the largest binding free-energy negative change at all cavities from all the independent cycles performed for each target–ligand complex. The generated data of all systems studied here follow the FAIR principles [46] and can be accessed and visualized at the MDdb Science Gateway at https://www.mddb.org with Study ID 690004.

3.1. PPARs Co-Crystallized Ligand Complexes Are Reproduced by the Blind Docking Protocol. The ample blind conformational sampling correctly predicted the biologically active LBD cavity for all the co-crystallized ligands in the positive control group with the lowest ΔG_b values in the corresponding target. The superposition of the crystal structure and the docked conformation reveals that the ligands are predicted to bind to the same site and maintain a similar pose as the ligand in the crystal structure in all cases (Figure 5), namely, ET1 for PPARα (RMSD = 5.016), D32 for PPARβ/δ (RMSD = 0.782), and CTI for PPARγ (RMSD = 5.059). This evidence suggests that the general pipeline employed in this study is reliable and produces accurate results.

3.2. Global Analysis of the Ligand Set and PPARs. The ΔG_b values for the blind docking results of the three isoforms of PPARs and some molecular components of the HB-ATV-8 nanoparticles (peptide Helix-Y^{12} and main lipids of the plasmatic membrane of *T. aquaticus*) are shown in Figure 6. Based on the statistical Z-score analysis done over the ligand set for each PPAR (columns), the Tzeax, Tzeax-13, and Tzeax-15 are the components of the HB-ATV-8 nanoparticles that have the most favorable thermodynamic interaction

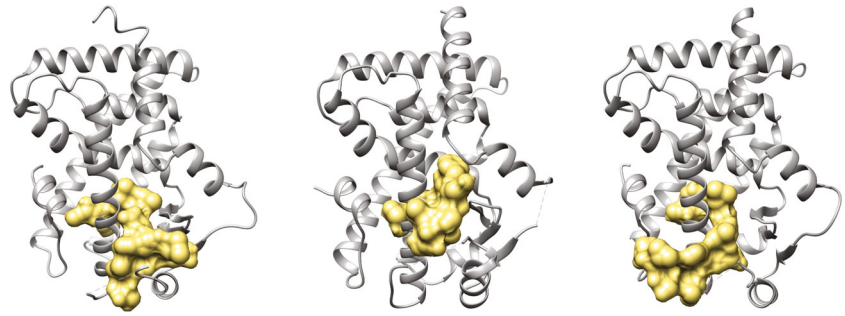

PPARα PPARβ/δ PPARγ

Figure 7: Ribbon diagrams of PPARα, PPARβ/δ, and PPARγ (grey) bound to surface diagram of peptide Helix-Y^{12} (gold).

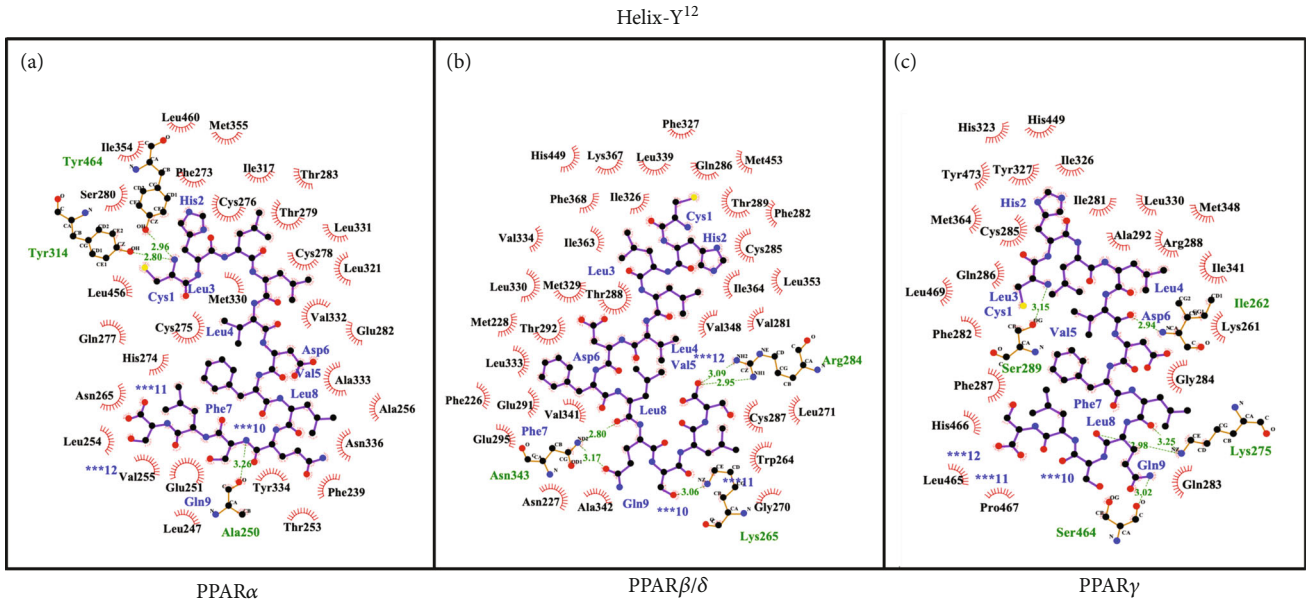

PPARα PPARβ/δ PPARγ

Figure 8: Interatomic interaction of peptide Helix-Y^{12} (label in blue) with (a) PPARα, (b) PPARβ/δ, and (c) PPARγ. Hydrogen bonds are indicated with green label and hydrophobic forces in black one.

with all three isoforms of PPARs, followed by peptide Helix-Y^{12} (Figure 6(a)). However, the interaction of the peptide with PPAR LBD shows more hydrogen bonds than that of the Tzeaxs. This result suggests a specific interaction between the PPARs and the peptide than the Tzeaxs under physiological conditions.

When the statistical Z-score analysis was performed on the target set for each ligand (rows), we found PPARα had the most favorable thermodynamic interaction with Helix-Y^{12} and Tzeax across the three isoforms. Meanwhile, PPARβ/δ had the most favorable thermodynamic interaction with Tzeax-13 and Tzeax-15 (Figure 6(b)). According to our analysis, the less favorable receptor for this set of ligands seems to be PPARγ. In this sense, PPARα LBD has an affinity for a broader range of saturated fatty acids than PPARγ and PPARβ/δ [47], explained by having the most lipophilic ligand-binding pocket of the three isoforms [48].

3.3. Helix-Y^{12} Forms a Stabilizing Hydrogen Bond Network with PPARs. Helix-Y^{12} is an amphipathic peptide that interacts with the whole Y-shaped ligand-binding pocket surface of the PPARs LBD, as shown in Figure 7. We found that a hydrogen bond network is formed between the PPARs and this peptide, although it involves different protein residues in each isoform.

Helix-Y^{12} makes three hydrogen bonds via Cys1 and Ser10 with residues Tyr314, Tyr464, and Ala250 of PPARα LBD (Figure 8(a)). There are also hydrophobic interactions involving β-sheets (13%) and H3 (30%). It should be noted that Helix-Y^{12} binds to PPARα LBD through hydrogen bonds in Tyr314 and Tyr464, which have previously been reported to interact with several PPARα ligands. PPARα crystallographic studies indicated that the interaction of ligands through Tyr464 and Tyr314 stabilizes the AF-2 helix, promoting the recruitment of coactivators [47, 49, 50]. Endogenous ligands (stearic and palmitic acid) and synthetic ligands (pemafibrate, saroglitazar, and GW7647) interact primarily with hydrophobic residues. Their carboxylic acid establishes a network of hydrogen bonds by common residues Tyr314, His440, Tyr 464, and Ser280. Synthetic ligands

Table 2: Main characteristics of Helix-Y^{12} interaction with PPARs.

	PPARα	PPARβ/δ	PPARγ
ΔG_b	−8.9	−7.9	−8.0
Interaction with Y-shaped ligand-binding pocket	Arm I, II, III[a], and X	Arm I, II, III and X[a]	Arm I, II, III[a], and X
Amino acid residues involved in H-bond (Receptor Helix-Y^{12})	Tyr314[b]–Cys1 Tyr464[b]–Cys1 Ala250–Ser10	Asn343–Leu8 Asn343–Gln9 Lys265–Ser10 Arg284–Ser10 (2x)	Ser289[b]–Cys1 Ile262–Val5 Lys275–Leu8 Lys275–Gln9 Ser464–Gln9
Hydrophobic contacts (mainly)	H3 (30%) H2′ (13.3%) H2′–H3 loop (13.3%) β2/β3 loop (10%)	H3 (29%) H5 (14%) H2′–H3 (11%) H7 (11%)	H3 (37%) H5 (15%) H12 (11%) H11–H12 (11%)
Advantages	Stablish two hydrogen bonds with residues of helix H12 important to LBD stabilization.	Hydrogen bonds are in Arm II and entrance.	Clamp surrounds H3, contacts with H12through a H-bond and several hydrophobic interactions, reaching loop H11–H12 from outside.

[a]Partial contact.
[b]Previously reported amino acids interacting with endogenous/exogenous ligands.

also interact through hydrogen bonds, involving other residues, such as Tyr334, Lys257, Cys275, Thr279, and Glu282 (ciprofibrate) and Ala333, Glu251, Leu331, Cys275, and Thr279 (pemafibrate) [50, 51]. Furthermore, several residues of PPARα that participate in the hydrophobic effect with the peptide correspond to those that interact with fatty acids (stearic and palmitic acid) and fibrates derivatives (pemafibrate and ciprofibrate). Isothermal titration calorimetry and fragment molecular orbital studies pointed out that the accumulation of weak hydrophobic contacts is important for the binding affinity of pemafibrate to PPARα LBD, as they confer a higher affinity for it compared with fenofibrate [51].

For PPARβ/δ LBD, Helix-Y^{12} also covers the entire Y-shaped ligand-binding pocket, but its contact with Arm X is minimal (Figure 7). Asn343, Lys265, and Arg284 interact via hydrogen bonds with Helix-Y^{12} residues Leu8, Gln9, Ser10, and Ser12 (Figure 8(b)). Hydrophobic contacts with H3 (29%), H5 (14%), loop H2′–H3 (11%), and H7 (11%) were also observed.

Finally, we show in Figure 7 that Helix-Y^{12} forms a clamp around H3 and reaches up to helix H12 of PPARγ. In this complex, the peptide is in Arm I, center, and partially in Arm III, leaving a binding-ligand pocket through Arms II and X. The interatomic analysis shows that Ile262, Lys275, Ser289, and Ser464 of PPARγ LBD interact with the peptide residues Cys1, Val5, Leu8, and Gln9 through hydrogen bonds (Figure 8(c)). In addition to these dipole–dipole attractive interactions, there are also hydrophobic contacts mainly with H3 (37%), H5 (15%), loop H11–H12 (11%), and H12 (11%). Of the amino acid residues that establish hydrogen bonds between Helix-Y^{12} and PPARγ, Ser289 has been reported in full agonists, such as rosiglitazone and MLR-20. The rest are in a region essential for LBD organization, such as the loops H2′–H3 and H11–H12.

Table 2 summarizes relevant characteristics observed in the interaction of Helix-Y^{12} and PPARs. Although Helix-Y^{12} does not show the highest ΔG_b values, it established interactions with amino acids reported from the Y-shaped ligand-binding pocket that happen with other ligands. Most of them are hydrophobic but some can make hydrogen bonds, related to the specificity for PPARs [50]. Helix-Y^{12} surrounds helix *H*3 of the PPAR LBD to a lesser or greater extent, occupying all three arms. In vitro studies have shown that peptide Helix-Y^{12} has biological effects on hepatocytes (in preparation). Altogether, these findings suggest that the peptide could be an exciting ligand that needs further studies to validate its interactions and a possible biological effect.

3.4. Tzeaxs Have the most Stable Interaction with PPARs. The interaction of PPARs LBD with Tzeax, Tzeax-13, and Tzeax-15 is shown in Figure 9. As previously mentioned, Tzeax, Tzeax-13, and Tzeax-15 have the most favorable thermodynamic change in free energy of binding with the three isoforms of PPARs from all molecules tested.

According to the ΔG_b values for the blind docking results, Tzeax shows a more favorable interaction with PPARα and PPARγ than the ligands employed in the co-crystallization with the protein, ET1 and CTI, respectively. This is not the case for PPARβ/δ, where ligand D32 stands out over the entire set of components of HB-ATV-8.

Another opposite trend is also apparent between PPARα and PPARγ with PPARβ/δ. Decreasing the aliphatic chain length of the Tzeaxs improves the interaction stability for the former, whereas increasing the length improves the interaction stability for the later. All other ligands are close to or significantly less negative than the set's ΔG_b mean value.

3.5. Tzeaxs Interact with the PPARs Mainly by Hydrophobic Contacts. As previously mentioned, we found that Tzeax,

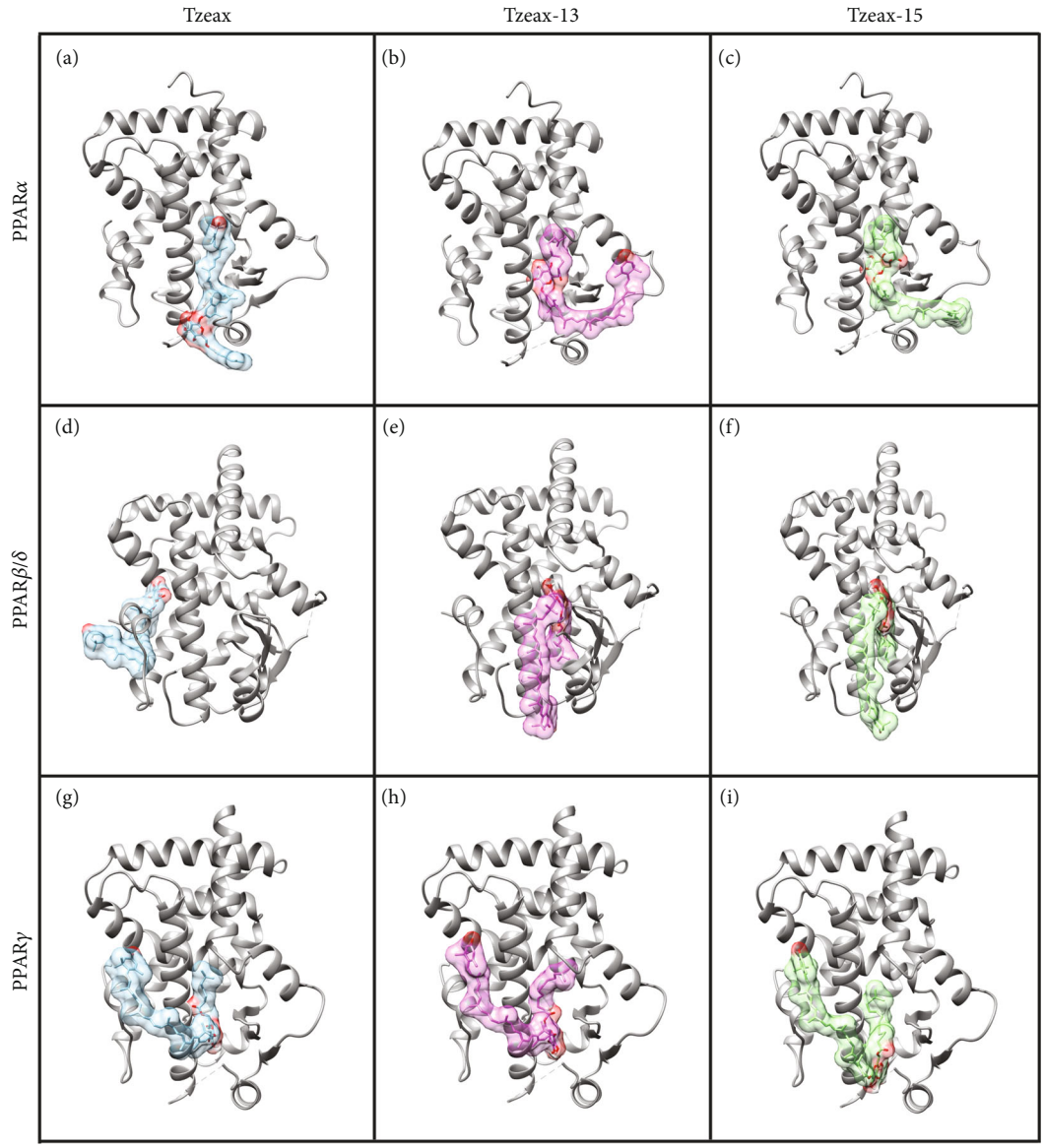

Figure 9: Ribbon diagrams of PPARα, PPARβ/δ, and PPARγ (grey) bound to surface/ribbon diagrams of (a, d, and g) Tzeax (blue), (b, e, and h) Tzeax-13 (pink), and (c, f, and i) Tzeax-15 (green).

Tzeax-13, and Tzeax-15 established contacts with the LBD PPARs, except for Tzeax and PPARβ/δ (Figure 9). For the Tzeax, the free polar ring of the zeaxanthin portion reaches Arm III of the ligand-binding pocket of PPARα, and the rest of the molecule passes through Arms II and X, leaving the fatty acid fraction on the outside (Figure 9(a)). However, all the contacts are due to the hydrophobic effect. They are mainly found in H3 (25%), loops (25%), and β-sheets (17%; Figure 10(a)). In contrast, the ester bond of Tzeax-13 located in the Arm II of the ligand-binding pocket of PPARα establishes hydrogen-bonds with the amide group of Tyr334 and Ala333 (Figures 9(b) and 10(b)). In addition to hydrogen bonds, there are hydrophobic contacts with H2′ (13%), H3 (21%), H5 (13%), β-sheets (17%), and loop H1–H2 (13%). On the other hand, Figure 10(c) shows how Tzeax-15 forms a direct hydrogen bond with Tyr334 of PPARα LBD, and hydrophobic contacts with H3 (23%), H5 (14%), and β-sheets (23%). Both Tzeax-13 and Tzeax-15 reach Arm III of the ligand-binding pocket of PPARα with the fatty acid portion; meanwhile, the zeaxanthin portion makes contact with Arm II and projects outside (Figures 9(b) and 9(c)). Tzeaxs present some observed hydrogen-bond interactions (Tyr334 and Ala333) and hydrophobic contacts (Cys275, Thr283, Leu321, and Val324) with fibrate derivatives, such as pemafibrate and ciprofibrate [50, 51].

In contrast to PPARα, Tzeax does not bind to the Y-shaped ligand-binding pocket of PPARβ/δ. Instead, it is located outside of the LBD, on the H11 and H12 helices (Figure 9(d)), consistent with the previous finding that long-chain fatty acids ($C > 20$) do not fit into the pocket [52]. However, when a short fatty acid is added to Tzeax, the interaction happens as follows: the glucoside ester of Tzeax-13 and Tzeax-15 establishes contact with PPARβ/δ

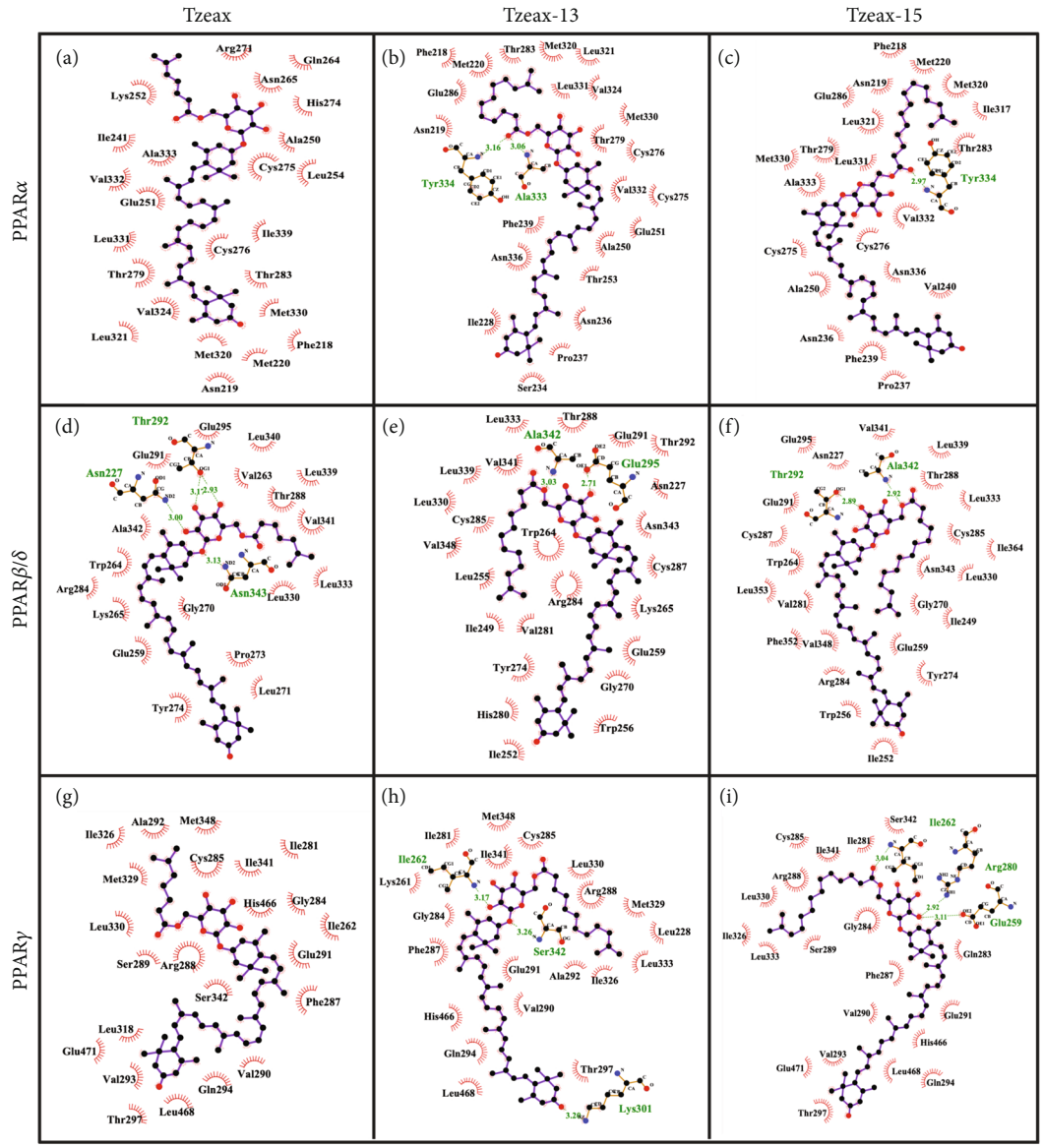

Figure 10: Interatomic interaction of thermozeaxanthins and PPAR-LBDs. Interatomic interaction of Tzeax with (a) PPARα, (d) PPARβ/δ, and (g) PPARγ, Tzeax-13 with (b) PPARα, (e) PPARβ/δ, and (h) PPARγ, and Tzeax-15 with (c) PPARα, (f) PPARβ/δ, and (i) PPARγ. All plots were generated using LigPlot. Labels in green correspond to residues involved in hydrogen bonds, and black one to those that interact by hydrophobic forces.

LBD through two hydrogen bonds at residues Ala342 and Glu295 (Tzeax-13; Figure 10(e)), and Thr292 and Ala342 (Tzeax-15; Figure 10(f)). In addition to hydrogen bonds, there are also hydrophobic contacts mainly with H3 (35%), H2′ (15%), and β-sheets (15%). Both Tzeax-13 and Tzeax-15 are in Arms II and III of the Y-shaped ligand-binding pocket of PPARβ/δ (Figures 9(e) and 9(f)). However, LBD of PPARβ/δ residues that make hydrogen bonds with Tzeax-13 and Tzeax-15 are different from those observed in eicosapentaenoic acid and GW2433; they make a network of hydrogen bonds via His323, His449, and Tyr473. Meanwhile, several residues (Arg284, Cys285, Leu339, and Val 348) interact with GW501515, a selective small-molecule [53], which are also observed in Tzeax-13 and Tzeax-15 interactions.

Figures 9(g) and 10(g) show how Tzeax interacts with PPARγ LBD in the same way as it does with PPARα, i.e., via hydrophobic contacts, with the exception that the interactions occur with H3 (55%), H4–H5 (18%), and H12 (9%). Tzeax can extend to Arms III, II, and X (Figure 9(g)). Meanwhile, the glucoside and fatty acid of the Tzeax-13 and Tzeax-15 are located in Arms II, III, and X of Y-shaped ligand-binding pocket, and zeaxanthin fraction surrounds LBD by H3, H4, and H12 (Figures 9(h) and 9(i)). In contrast to Tzeax, three hydrogen bonds were observed when the aliphatic chain increased from 7 to 12 carbons, namely, Tzeax13. Glucoside fraction of Tzeax-13 makes hydrogen bonds with residues Ile262 and Ser342 and the polar ring in the opposite site with residue Lys301 (H3; Figure 10(h)). A constant hydrophobic core interaction with H3 (43%)

and H5 (17%) was also found. Similarly, the glucoside ester of Tzeax-15 establishes hydrogen bonds to H3 through Arg280 and loop H2'–H3 (Glu259 and Ile262) of PPARγ LBD, establishing an interaction with Arm X (Figure 10(i)). Hydrophobic interactions with H3 (57%) and H5 (13%) are also present. These findings suggest that Tzeax-13 and Tzeax-15 could be partial agonists of PPARγ because they share similar molecular interactions through some amino acid residues observed in partial agonists, such as amorfrutin, MLR-24, nTZDpa, and BVT.13 [54]. It has been recognized that there are different mechanisms of stabilization of LBD between full and partial agonists, explaining the differences in the grade of transactivation. Rosiglitazone and MRL-20, two full agonists, stabilize H3 and H12 helices of PPARγ LBD through hydrogen bonds via Tyr473 and His449 [55]. Meanwhile, partial agonists, such as amorfrutin, MLR-24, nTZDpa, and BVT.13, tend to stabilize helix H3 and the β-sheet region, but at the same time destabilize helix H12. The binding to helix H3 and β-sheet through hydrogen bonds via Ser342 and Arg388 along with several hydrophobic contacts, including Ile341 (β-sheet) and Cys285 (H3), enables its stabilization [54].

HB-ATV-8 formulation has several advantages since it comprises nanomicellar structures around 10 nm in diameter, composed of membrane lipids of *T. aquaticus* and the peptide Helix-Y^{12}. The small size of micelles is achieved because the peptide is able to modify the diameter of micelles (~100 nm) formed by pure lipids [56]. It has been shown that this kind of nanostructure is stable in terms of thermodynamics and kinetics [57, 58]. In addition, nanomicelles with amphipathic peptides are efficient delivery systems and promoting transport across membranes [59, 60]. Additionally, lipid–peptide complexes are convenient for maintaining structural stability and lesser degradation of peptides [61].

Finally, it is important to consider that a ligand can interact with more than one of the members of PPARs (dual agonist and pan agonist), but the affinity and the strength of activation depend on the molecular interactions established with each receptor. Each ligand promotes a unique conformational change, leading to differential pattern of coregulator recruitment, which in turn might cause gene selective effects [62]. Therefore, further understanding of the synergistic or antagonistic effects of HB-ATV-8 components as PPARs ligands is necessary to discard the possible disadvantage of administrating more than one ligand.

4. Conclusions

In the present study, we use blind molecular docking to show that the peptide Helix-Y^{12}, Tzeax, Tzeax-13, and Tzeax-15, components of HB-ATV-8, favorably interact with the PPARs LBD. Although the interaction is mediated mainly by hydrophobic contacts, Helix-Y^{12}, Tzeax-13, and Tzeax-15, share specific hydrogen bond interactions previously reported for known PPAR ligands. The Helix-Y^{12} fills the entire Y-shaped ligand-binding pocket of PPARα and PPARγ, but its contact with Arm III is partial. In the case of PPARβ/δ, there is a slight difference; the peptide establishes partial contact with Arm II. In contrast, Tzeaxs are constantly located in Arms II and III of the Y-shaped ligand-binding pockets of PPARα and PPARγ. Meanwhile, in PPARβ/δ they only occupy Arm II.

Previous study in our laboratory has demonstrated that the nasal administration of HB-ATV-8, containing Tzeaxs and Helix-Y^{12}, reduces hypertriglyceridemia and vascular and hepatic lesions, including fibrosis, induced by a high-fat diet enriched with cholesterol in pigs and rabbits [29, 30]. In this line, PPARα agonists are useful drugs for reducing serum triglycerides [63]. It is well known that PPARα activated with fibrates and its derivatives reduce triglycerides-rich lipoproteins promoting fatty acids uptake and oxidation and increasing lipoprotein lipase activity [15, 64]. Preclinical [62, 65–67] and clinical [68–70] studies demonstrated that PPAR has an important role in NAFLD and non-alcoholic fatty steatohepatitis (NASH). PPARα agonist counteracted dietary-induced NASH through PPARα transrepression of signaling pathways that participate activator protein-1 and NF-κB [66]. On the other hand, activation of PPARβ/δ with GW501516 leads to a reduction of hepatic fat accumulation and inflammation. In NAFLD/NASH animal models, elafibranor, a dual agonist PPARα–β/δ, reduces hepatic steatosis, inflammation, and fibrosis [71, 72]. As well as patients with NASH, dyslipidemia, and prediabetic, elafibranor reduces plasma lipids and hepatic inflammation biomarkers [73, 74]. GFT505, a dual PPARα–β/δ, demonstrated liver-protective effects on steatosis, inflammation, and fibrosis in animal models of NAFLD/NASH and liver fibrosis [75]. Therefore, activating more than one PPAR family member by a suitable exogenous ligand (dual- or pan-agonist) could represent an effective therapy against several metabolic alterations, such as hypertriglyceridemia, NAFLD, even fibrosis, and inflammation. Furthermore, according to our molecular docking results, the nanoparticle components, such as Helix-Y^{12} and Tzeax, might activate both PPARα and PPARβ/δ, which would help us explain the protective effects against hypertriglyceridemia, vascular, and liver lesions.

Data Availability

The generated data of all systems studied here follow the FAIR principles and can be accessed and visualized at the MDdb Science Gateway at https://www.md-db.org with Study ID 690004.

Conflicts of Interest

The author(s) declare(s) that they have no conflicts of interest.

Acknowledgments

All the results reported here were obtained at the bmdHPC computing resources of the Biomolecular Diversity Lab (http://tripplab.com) at CINVESTAV Unidad Monterrey, México, funded by the Consejo Nacional de Ciencia y Tecnología México (grant number 132376 to M. C.-T.).

References

[1] J. Berger and D. E. Moller, "The mechanisms of action of PPARs," *Annual Review of Medicine*, vol. 53, no. 1, pp. 409–435, 2002.

[2] R. A. Daynes and D. C. Jones, "Emerging roles of PPARS in inflammation and immunity," *Nature Reviews Immunology*, vol. 2, no. 10, pp. 748–759, 2002.

[3] L. Han, W.-J. Shen, S. Bittner, F. B. Kraemer, and S. Azhar, "PPARs: regulators of metabolism and as therapeutic targets in cardiovascular disease. Part II: PPAR-β/δ and PPAR-γ," *Future Cardiology*, vol. 13, no. 3, pp. 279–296, 2017.

[4] N. Marx, T. Bourcier, G. K. Sukhova, P. Libby, and J. Plutzky, "PPARγ activation in human endothelial cells increases plasminogen activator inhibitor type-1 expression," *Arteriosclerosis, Thrombosis, and Vascular Biology*, vol. 19, no. 3, pp. 546–551, 1999.

[5] R. Mukherjee, L. Jow, G. E. Croston, and J. R. Paterniti, "Identification, characterization, and tissue distribution of human peroxisome proliferator-activated receptor (PPAR) isoforms PPARγ2 versus PPAR γ1 and activation with retinoid X receptor agonists and antagonists," *Journal of Biological Chemistry*, vol. 272, no. 12, pp. 8071–8076, 1997.

[6] A. J. Vidal-Puig, R. V. Considine, M. Jimenez-Liñan et al., "Peroxisome proliferator-activated receptor gene expression in human tissues. Effects of obesity, weight loss, and regulation by insulin and glucocorticoids," *Journal of Clinical Investigation*, vol. 99, no. 10, pp. 2416–2422, 1997.

[7] G. Chinetti, J.-C. Fruchart, and B. Staels, "Peroxisome proliferator-activated receptors (PPARs): nuclear receptors at the crossroads between lipid metabolism and inflammation," *Inflammation Research*, vol. 49, no. 10, pp. 497–505, 2000.

[8] H. Higashiyama, A. N. Billin, Y. Okamoto, M. Kinoshita, and S. Asano, "Expression profiling of peroxisome proliferator-activated receptor-delta (PPAR-delta) in mouse tissues using tissue microarray," *Histochemistry and Cell Biology*, vol. 127, no. 5, pp. 485–494, 2007.

[9] D. J. Kojetin and T. P. Burris, "Small molecule modulation of nuclear receptor conformational dynamics: implications for function and drug discovery," *Molecular Pharmacology*, vol. 83, no. 1, pp. 1–8, 2013.

[10] S. Sauer, "Ligands for the nuclear peroxisome proliferator-activated receptor gamma," *Trends in Pharmacological Sciences*, vol. 36, no. 10, pp. 688–704, 2015.

[11] M. Ricote and C. Glass, "PPARs and molecular mechanisms of transrepression," *Biochimica et Biophysica Acta*, vol. 1771, no. 8, pp. 926–935, 2007.

[12] M. Bloch, A. Prock, F. Paonessa et al., "High-mobility group A1 protein: a new coregulator of peroxisome proliferator-activated receptor-mediated transrepression in the vasculature," *Circulation Research*, vol. 110, no. 3, pp. 394–405, 2012.

[13] N. Tanaka, T. Aoyama, S. Kimura, and F. J. Gonzalez, "Targeting nuclear receptors for the treatment of fatty liver disease," *Pharmacology and Therapeutics*, vol. 179, pp. 142–157, 2017.

[14] W. Wahli and L. Michalik, "PPARs at the crossroads of lipid signaling and inflammation," *Trends in Endocrinology and Metabolism*, vol. 23, no. 7, pp. 351–363, 2012.

[15] K. Schoonjans, J. Peinado-Onsurbe, A. M. Lefebvre et al., "PPARalpha and PPARgamma activators direct a distinct tissue-specific transcriptional response via a PPRE in the lipoprotein lipase gene," *The EMBO Journal*, vol. 15, no. 19, pp. 5336–5348, 1996.

[16] C. Maccallini, A. Mollica, and R. Amoroso, "The positive regulation of eNOS signaling by PPAR agonists in cardiovascular diseases," *American Journal of Cardiovascular Drugs*, vol. 17, no. 4, pp. 273–281, 2017.

[17] R. M. Touyz and E. L. Schiffrin, "Peroxisome proliferator-activated receptors in vascular biology-molecular mechanisms and clinical implications," *Vascular Pharmacology*, vol. 45, no. 1, pp. 19–28, 2006.

[18] H.-C. Lin, C.-K. Lii, A.-H. Lin et al., "Docosahexaenoic acid inhibits TNFα-induced ICAM-1 expression by activating PPARα and autophagy in human endothelial cells," *Food and Chemical Toxicology*, vol. 134, article 110811, 2019.

[19] M. Gholizadeh, S. A. G. Saeedy, P. B. Roodi, and A. Saedisomeolia, "The association between zinc and endothelial adhesion molecules ICAMs and VCAM-1 and nuclear receptors PPAR-α and PPAR-γ: a systematic review on cell culture, animal and human studies," *Microvascular Research*, vol. 138, p. 104217, 2021.

[20] A. Christofides, E. Konstantinidou, C. Jani, and V. A. Boussiotis, "The role of peroxisome proliferator-activated receptors (PPAR) in immune responses," *Metabolism*, vol. 114, p. 154338, 2021.

[21] A. D. Patterson, Y. M. Shah, T. Matsubara, K. W. Krausz, and F. J. Gonzalez, "Peroxisome proliferator-activated receptor alpha induction of uncoupling protein 2 protects against acetaminophen-induced liver toxicity," *Hepatology*, vol. 56, no. 1, pp. 281–290, 2012.

[22] X. Ma, D. Wang, W. Zhao, and L. Xu, "Deciphering the roles of PPARγ in adipocytes via dynamic change of transcription complex," *Frontiers in Endocrinology*, vol. 9, p. 473, 2018.

[23] C. Weidner, S. J. Wowro, A. Freiwald et al., "Amorfrutin B is an efficient natural peroxisome proliferator-activated receptor gamma (PPARγ) agonist with potent glucose-lowering properties," *Diabetologia*, vol. 56, no. 8, pp. 1802–1812, 2013.

[24] D. F. Klessig, M. Tian, and H. W. Choi, "Multiple targets of salicylic acid and its derivatives in plants and animals," *Frontiers in Immunology*, vol. 7, p. 206, 2016.

[25] P. Xu, Y. Zhai, and J. Wang, "The role of PPAR and its cross-talk with CAR and LXR in obesity and atherosclerosis," *International Journal of Molecular Sciences*, vol. 19, no. 4, p. 1260, 2018.

[26] V. Souza-Mello, B. M. Gregório, F. S. Cardoso-de Lemos, L. de Carvalho, M. B. Aguila, and C. A. Mandarim-de Lacerda, "Comparative effects of telmisartan, sitagliptin and metformin alone or in combination on obesity, insulin resistance, and liver and pancreas remodelling in C57BL/6 mice fed on a very high-fat diet," *Clinical Science*, vol. 119, no. 6, pp. 239–250, 2010.

[27] N. Hennuyer, I. Duplan, C. Paquet et al., "The novel selective PPARα modulator (SPPARMα) pemafibrate improves dyslipidemia, enhances reverse cholesterol transport and decreases inflammation and atherosclerosis," *Atherosclerosis*, vol. 249, pp. 200–208, 2016.

[28] D. M. Corigliano, R. Syed, S. Messineo et al., "Indole and 2,4-thiazolidinedione conjugates as potential anticancer modulators," *PeerJ*, vol. 6, p. e5386, 2018.

[29] R. Gutiérrez-Vidal, B. Delgado-Coello, K. M. Méndez-Acevedo, S. Calixto-Tlacomulco, S. Damián-Zamacona, and J. Mas-Oliva, "Therapeutic intranasal vaccine HB-ATV-8 prevents atherogenesis and non-alcoholic fatty liver disease in a pig model of atherosclerosis," *Archives of Medical Research*, vol. 49, no. 7, pp. 456–470, 2018.

[30] V. García-González, B. Delgado-Coello, A. Pérez-Torres, and J. Mas-Oliva, "Reality of a vaccine in the prevention and treatment of atherosclerosis," *Archives of Medical Research*, vol. 46, no. 5, pp. 427–437, 2015.

[31] C. Yang, C. Zhang, Z. Wang, Z. Tang, H. Kuang, and A.-N. Kong, "Corynoline isolated from Corydalis bungeana Turcz. exhibits anti-inflammatory effects via modulation of Nfr2 and MAPKs," *Molecules*, vol. 21, no. 8, p. 975, 2016.

[32] J. Karppi, S. Kurl, J. A. Laukkanen, T. H. Rissanen, and J. Kauhanen, "Plasma carotenoids are related to intima—media thickness of the carotid artery wall in men from eastern Finland," *Journal of Internal Medicine*, vol. 270, no. 5, pp. 478–485, 2011.

[33] L. Verschuren, P. Y. Wielinga, W. van Duyvenvoorde et al., "A dietary mixture containing fish oil, resveratrol, lycopene, catechins, and vitamins E and C reduces atherosclerosis in transgenic mice," *The Journal of Nutrition*, vol. 141, no. 5, pp. 863–869, 2011.

[34] X. Yang, Y. Li, Y. Li et al., "Oxidative stress-mediated atherosclerosis: mechanisms and therapies," *Frontiers in Physiology*, vol. 8, p. 600, 2017.

[35] P. Marchio, S. Guerra-Ojeda, J. M. Vila, M. Aldasoro, V. M. Victor, and M. D. Mauricio, "Targeting early atherosclerosis: a focus on oxidative stress and inflammation," *Oxidative Medicine and Cellular Longevity*, vol. 2019, 2019.

[36] H. M. Berman, J. Westbrook, Z. Feng et al., "The protein data bank," *Nucleic Acids Research*, vol. 28, no. 1, pp. 235–242, 2000.

[37] E. F. Pettersen, T. D. Goddard, C. C. Huang et al., "UCSF Chimera—a visualization system for exploratory research and analysis," *Journal of Computational Chemistry*, vol. 25, no. 13, pp. 1605–1612, 2004.

[38] M. V. Shapovalov and R. L. Dunbrack, "A smoothed backbone-dependent Rotamer library for proteins derived from adaptive kernel density estimates and regressions," *Structure*, vol. 19, no. 6, pp. 844–858, 2011.

[39] V. García-González and J. Mas-Oliva, "Amyloid fibril formation of peptides derived from the C-terminus of CETP modulated by lipids," *Biochemical and Biophysical Research Communications*, vol. 434, no. 1, pp. 54–59, 2013.

[40] A. Herrera-Rodulfo, M. Andrade-Medina, and M. Carrillo-Tripp, "Repurposing Drugs as Potential Therapeutics for the SARS-Cov-2 Viral Infection: Automatizing a Blind Molecular Docking High-throughput Pipeline," in *Molecular Docking*, E. S. Istifli, Ed., pp. 119–148, IntechOpen, Rijeka, 2022.

[41] Y. Liu, M. Grimm, W.-T. Dai, M.-C. Hou, Z.-X. Xiao, and Y. Cao, "CB-dock: a web server for cavity detection-guided protein–ligand blind docking," *Acta Pharmacologica Sinica*, vol. 41, pp. 138–144, 2019.

[42] O. Trott and A. J. Olson, "AutoDock Vina: improving the speed and accuracy of docking with a new scoring function, efficient optimization, and multithreading," *Journal of Computational Chemistry*, vol. 31, no. 2, pp. 455–461, 2010.

[43] Y. Cao and L. Li, "Improved protein–ligand binding affinity prediction by using a curvature dependent surface-area model," *Bioinformatics*, vol. 30, no. 12, pp. 1674–1680, 2014.

[44] A. C. Wallace, R. A. Laskowski, and J. M. Thornton, "LIGPLOT: a program to generate schematic diagrams of protein-ligand interactions," *Protein Engineering Design and Selection*, vol. 8, no. 2, pp. 127–134, 1995.

[45] Y. Zhang and J. Skolnick, "TM-align: a protein structure alignment algorithm based on the TM-score," *Nucleic Acids Research*, vol. 33, no. 7, pp. 2302–2309, 2005.

[46] M. D. Wilkinson, M. Dumontier, I. J. J. Aalbersberg, G. Appleton, M. Axton, and A. Baak, "The FAIR guiding principles for scientific data management and stewardship," *Scientific Data*, vol. 3, p. 160018, 2016.

[47] H. E. Xu, M. H. Lambert, V. G. Montana et al., "Structural determinants of ligand binding selectivity between the peroxisome proliferator-activated receptors," *Proceedings of the National Academy of Sciences of the United States of America*, vol. 98, no. 24, pp. 13919–13924, 2001.

[48] G. S. Harmon, M. T. Lam, and C. K. Glass, "PPARs and lipid ligands in inflammation and metabolism," *Chemical Reviews*, vol. 111, no. 10, pp. 6321–6340, 2011.

[49] Y.-J. Wang, S.-C. Lee, C.-H. Hsu, Y.-H. Kuo, C.-C. Yang, and F.-J. Lin, "Antcins, triterpenoids from Antrodia cinnamomea, as new agonists for peroxisome proliferator-activated receptor α," *Journal of Food and Drug Analysis*, vol. 27, no. 1, pp. 295–304, 2019.

[50] S. Kamata, T. Oyama, K. Saito et al., "PPARα ligand-binding domain structures with endogenous fatty acids and fibrates," *iScience*, vol. 23, no. 11, p. 101727, 2020.

[51] M. Kawasaki, A. Kambe, Y. Yamamoto et al., "Elucidation of molecular mechanism of a selective PPARα modulator, pemafibrate, through combinational approaches of X-ray crystallography, thermodynamic analysis, and first-principle calculations," *International Journal of Molecular Sciences*, vol. 21, no. 1, p. 361, 2020.

[52] H. E. Xu, M. H. Lambert, V. G. Montana et al., "Molecular recognition of fatty acids by peroxisome proliferator-activated receptors," *Molecular Cell*, vol. 3, no. 3, pp. 397–403, 1999.

[53] C.-C. Wu, T. J. Baiga, M. Downes et al., "Structural basis for specific ligation of the peroxisome proliferator-activated receptor δ," *Proceedings of the National Academy of Sciences of the United States of America*, vol. 114, no. 13, pp. E2563–E2570, 2017.

[54] J. C. de Groot, C. Weidner, J. Krausze et al., "Structural characterization of amorfrutins bound to the peroxisome proliferator-activated receptor γ," *Journal of Medicinal Chemistry*, vol. 56, no. 4, pp. 1535–1543, 2013.

[55] J. B. Bruning, M. J. Chalmers, S. Prasad et al., "Partial agonists activate PPARγ using a helix 12 independent mechanism," *Structure*, vol. 15, no. 10, pp. 1258–1271, 2007.

[56] V. García-González, N. Gutiérrez-Quintanar, P. Mendoza-Espinosa, P. Brocos, A. Piñeiro, and J. Mas-Oliva, "Key structural arrangements at the C-terminus domain of CETP suggest a potential mechanism for lipid-transfer activity," *Journal of Structural Biology*, vol. 186, no. 1, pp. 19–27, 2014.

[57] A. Bose, D. Roy Burman, B. Sikdar, and P. Patra, "Nanomicelles: types, properties and applications in drug delivery," *IET Nanobiotechnology*, vol. 15, no. 1, pp. 19–27, 2021.

[58] V. P. Torchilin, "Micellar nanocarriers: pharmaceutical perspectives," *Pharmaceutical Research*, vol. 24, no. 1, pp. 1–16, 2007.

[59] S. M. Tawfik, S. Azizov, M. R. Elmasry, M. Sharipov, and Y.-I. Lee, "Recent advances in nanomicelles delivery systems," *Nanomaterials*, vol. 11, no. 1, p. 70, 2020.

[60] M. J. Mitchell, M. M. Billingsley, R. M. Haley, M. E. Wechsler, N. A. Peppas, and R. Langer, "Engineering precision

nanoparticles for drug delivery," *Nature Reviews Drug Discovery*, vol. 20, no. 2, pp. 101–124, 2021.

[61] V. Sethi, I. Rubinstein, A. Kuzmis, H. Kastrissios, J. Artwohl, and H. Onyuksel, "Novel, biocompatible, and disease modifying VIP nanomedicine for rheumatoid arthritis," *Molecular Pharmaceutics*, vol. 10, no. 2, pp. 728–738, 2013.

[62] J.-C. Fruchart, "Pemafibrate (K-877), a novel selective peroxisome proliferator-activated receptor alpha modulator for management of atherogenic dyslipidaemia," *Cardiovascular Diabetology*, vol. 16, no. 1, p. 124, 2017.

[63] B. Staels, J. Dallongeville, J. Auwerx, K. Schoonjans, E. Leitersdorf, and J. C. Fruchart, "Mechanism of action of fibrates on lipid and lipoprotein metabolism," *Circulation*, vol. 98, no. 19, pp. 2088–2093, 1998.

[64] V. Dubois, J. Eeckhoute, P. Lefebvre, and B. Staels, "Distinct but complementary contributions of PPAR isotypes to energy homeostasis," *Journal of Clinical Investigation*, vol. 127, no. 4, pp. 1202–1214, 2017.

[65] A. Montagner, A. Polizzi, E. Fouché et al., "Liver PPARα is crucial for whole-body fatty acid homeostasis and is protective against NAFLD," *Gut*, vol. 65, no. 7, pp. 1202–1214, 2016.

[66] M. Pawlak, P. Lefebvre, and B. Staels, "Molecular mechanism of PPARα action and its impact on lipid metabolism, inflammation and fibrosis in non-alcoholic fatty liver disease," *Journal of Hepatology*, vol. 62, no. 3, pp. 720–733, 2015.

[67] M. A. Abdelmegeed, S.-H. Yoo, L. E. Henderson, F. J. Gonzalez, K. J. Woodcroft, and B.-J. Song, "PPARα expression protects male mice from high fat-induced nonalcoholic fatty liver," *The Journal of Nutrition*, vol. 141, no. 4, pp. 603–610, 2011.

[68] S. Francque, A. Verrijken, S. Caron et al., "PPARα gene expression correlates with severity and histological treatment response in patients with non-alcoholic steatohepatitis," *Journal of Hepatology*, vol. 63, no. 1, pp. 164–173, 2015.

[69] Y. Seko, K. Yamaguchi, A. Umemura et al., "Effect of pemafibrate on fatty acid levels and liver enzymes in non-alcoholic fatty liver disease patients with dyslipidemia: a single-arm, pilot study," *Hepatology Research*, vol. 50, no. 12, pp. 1328–1336, 2020.

[70] Y. Sasaki, M. Asahiyama, T. Tanaka et al., "Pemafibrate, a selective PPARα modulator, prevents non-alcoholic steatohepatitis development without reducing the hepatic triglyceride content," *Scientific Reports*, vol. 10, no. 1, p. 7818, 2020.

[71] L. Tong, L. Wang, S. Yao et al., "PPARδ attenuates hepatic steatosis through autophagy-mediated fatty acid oxidation," *Cell Death and Disease*, vol. 10, no. 3, p. 197, 2019.

[72] X. Li, J. Li, X. Lu et al., "Treatment with PPARδ agonist alleviates non-alcoholic fatty liver disease by modulating glucose and fatty acid metabolic enzymes in a rat model," *International Journal of Molecular Medicine*, vol. 36, no. 3, pp. 767–775, 2015.

[73] V. Ratziu, S. A. Harrison, S. Francque et al., "Elafibranor, an agonist of the peroxisome proliferator–activated receptor–α and –δ, induces resolution of nonalcoholic steatohepatitis without fibrosis worsening," *Gastroenterology*, vol. 150, no. 5, pp. 1147–1159.e5, 2016.

[74] B. Cariou, Y. Zaïr, B. Staels, and E. Bruckert, "Effects of the new dual PPAR α/δ agonist GFT505 on lipid and glucose homeostasis in abdominally obese patients with combined dyslipidemia or impaired glucose metabolism," *Diabetes Care*, vol. 34, no. 9, pp. 2008–2014, 2011.

[75] B. Staels, A. Rubenstrunk, B. Noel et al., "Hepatoprotective effects of the dual peroxisome proliferator-activated receptor alpha/delta agonist, GFT505, in rodent models of nonalcoholic fatty liver disease/nonalcoholic steatohepatitis," *Hepatology*, vol. 58, no. 6, pp. 1941–1952, 2013.

[76] W. Tian, C. Chen, X. Lei, J. Zhao, and J. Liang, "CASTp 3.0: computed atlas of surface topography of proteins," *Nucleic Acids Research*, vol. 46, no. W1, pp. W363–W367, 2018.